Modeling Approach to Eliminate the Need to Separate Arterial Plasma in Oxygen-15 Inhalation Positron Emission Tomography

Hidehiro Iida, Terry Jones and Shuichi Miura

Research Institute for Brain and Blood Vessels, Akita, Japan and MRC Cyclotron Unit, Hammersmith Hospital, London, United Kingdom

A mathematical model has been developed to predict the arterial metabolite concentration curve using the whole blood radioactivity curve in positron emission tomography (PET) during $^{15}O_2$ inhalation. Production of arterial $H_2{}^{15}O$ due to aerobic metabolism in the body was modeled as a single rate constant, which was determined from 200 steady-state values of plasma and whole blood concentrations recorded during continuous inhalation of $^{15}O_2$ and $C^{15}O_2$. Comparison of this method in eight $^{15}O_2$ inhalation studies (four at rest and four during motor stimulation) performed on four subjects resulted in: (1) arterial $H_2{}^{15}O$ curves that were well matched in shape to those measured by the frequent plasma separation and (2) cerebral metabolic rate of oxygen ($CMRO_2$) and cerebral blood flow (CBF) were consistent with those obtained by the frequent plasma separation procedure (maximum difference was 3%). An error sensitivity analysis was also performed and demonstrated that errors expected in this modeling approach caused only negligible errors in $CMRO_2$ and CBF estimates. Thus, the arterial $H_2{}^{15}O$ concentration curve can be accurately predicted using the whole blood time-activity curve; hence, plasma separation can be avoided in $^{15}O_2$ inhalation PET.

J Nucl Med 1993; 34:1333–1340

Regional cerebral metabolic rate of oxygen ($CMRO_2$) can be measured using positron emission tomography (PET) and a short period of inhalating ^{15}O-labeled oxygen ($^{15}O_2$) (*1–4*). Simultaneous determination of $CMRO_2$ and cerebral blood flow (CBF) is also possible with single dynamic PET scanning during $^{15}O_2$ inhalation (*5–7*). These determinations are based on measurements of ^{15}O-labeled water (recirculating water, $H_2{}^{15}O$) and $^{15}O_2$ concentrations in arterial blood and a dynamic (or integral) measurement of regional radioactivity concentration in the brain using PET.

Received Dec. 21, 1992; revision accepted Apr. 1, 1993.

For correspondence or reprints contact: Dr. Hidehiro Iida, DSc, Department of Radiology and Nuclear Medicine, Research Institute for Brain and Blood Vessels, 6–10 Senshu-kubota Machi, Akita City, Akita 010, Japan.

Previously, arterial $H_2{}^{15}O$ and $^{15}O_2$ concentrations were measured by continuously monitoring radioactivity concentration in both whole blood and in plasma during the $^{15}O_2$ PET scanning. This, however, requires frequent plasma separation (*2,3*) or use of an on-line plasma separator (*7–9*) during the $^{15}O_2$ PET scan, which is labor-intensive. The purpose of the present study is to develop a method that predicts arterial $H_2{}^{15}O$ and $^{15}O_2$ concentration curves using the whole blood radioactivity concentration curve. It relies on the use of a common rate constant for $H_2{}^{15}O$ production in arterial blood and hence eliminates the need for plasma separation in a $^{15}O_2$ PET study. In order to test the validity of this method, it was compared in a series of $^{15}O_2$ PET studies performed on healthy volunteers with the standard complete blood sampling procedure of a $^{15}O_2$ inhalation PET study. This involved careful measuring of arterial $^{15}O_2$ and $H_2{}^{15}O$ concentrations by frequent plasma separation and correcting for delay and dispersion (*10,11*). We also employed error sensitivity analysis to confirm the stability of this technique.

THEORY

Prediction of Recirculating Water in Arterial Blood

The process for arterial $H_2{}^{15}O$ production in the body due to the aerobic metabolism was approximated by a single rate constant, k [min^{-1}]. The arterial $H_2{}^{15}O$ concentration increases and decreases in proportion to the arterial $^{15}O_2$ concentration. The differential equation for arterial $H_2{}^{15}O$ concentration (*12*) can therefore be expressed as:

$$\frac{dA_w(t)}{dt} = k \cdot A_o(t) - \lambda \cdot A_w(t). \qquad \text{Eq. 1}$$

(See Table 1 for glossary of terms.) The arterial whole blood concentration is a sum of arterial $H_2{}^{15}O$ and $^{15}O_2$ concentrations:

$$A_t(t) = A_o(t) + A_w(t). \qquad \text{Eq. 2}$$

Steady-State

When gaseous $^{15}O_2$ is inhaled to reach a steady-state, the radioactivity concentration in the whole body (and in the

TABLE 1
Glossary of Terms

$A_o(t)$ [Bq/ml]	Concentration of ^{15}O-labeled oxygen in the arterial blood during the $^{15}O_2$ inhalation study.
$A_w(t)$ [Bq/ml]	Concentration of ^{15}O-labeled water in the arterial blood during the $^{15}O_2$ inhalation study.
$A_t(t)$ [Bq/ml]	Whole blood radioactivity concentration during the $^{15}O_2$ inhalation study.
A(t) [Bq/ml]	Whole blood radioactivity concentration during the $C^{15}O_2$ inhalation study.
A_o [Bq/ml]	Blood $^{15}O_2$ concentration at steady state during $^{15}O_2$ inhalation.
A_w [Bq/ml]	Blood $H_2{}^{15}O$ concentration at steady state during $^{15}O_2$ inhalation.
A_t [Bq/ml]	Total blood radioactivity concentration at steady state during $^{15}O_2$ inhalation.
k [1/min]	Production rate constant of ^{15}O-labeled water in the arterial blood.
λ [1/min]	Decay constant of ^{15}O.
Δt [sec]	Delay of ^{15}O-labeled water appearance in the arterial blood.
K_1^o [1/min]	Regional influx rate constant of ^{15}O-labeled oxygen which is proportional to $CMRO_2$.
K_1^w [1/min]	Regional influx rate constant of ^{15}O-labeled water which is proportional to CBF.
V_d [ml/ml]	Regional distribution volume of water (= K_1^w/k_2^w).
k_2^w [1/min]	Regional outflux rate constant of ^{15}O-labeled water which is expressed as K_1^w divided by V_d.
V_B [ml/ml]	Regional cerebral blood volume.
$\otimes$	Convolution integral.

blood) reaches equilibrium, and the net production of metabolized water, left side of the Equation 1, becomes zero:

$$\frac{dA_w(t)}{dt} = 0. \qquad \text{Eq. 3}$$

Equations 1, 2 and 3 give

$$\left[\frac{A_w}{A_t}\right]^{t \text{ at equilibrium}} = \frac{k}{k+\lambda} \qquad \text{Eq. 4}$$

hence, the production rate constant of $H_2{}^{15}O$ as:

$$k = \lambda \cdot \left(\frac{A_w}{A_t}\right) \Big/ \left(1 - \frac{A_w}{A_t}\right). \qquad \text{Eq. 5}$$

The ratio of arterial $H_2{}^{15}O$-to-whole blood radioactivity concentrations, (A_w/A_t), has been calculated for 200 steady-state studies (*13*) randomly selected from studies done in MRC Cyclotron Unit, Hammersmith Hospital, London (*14–16*). This analysis yielded

$$\frac{A_w}{A_t} = 0.176 \pm 0.036 \qquad \text{Eq. 6a}$$

and

$$\frac{A_o}{A_t} = 0.824 \pm 0.036, \qquad \text{Eq. 6b}$$

where values were noted as mean ± 1 s.d. Hence, the production rate constant, k, was obtained as:

$$k = 0.0722 \pm 0.0126 \text{ min}^{-1}. \qquad \text{Eq. 7}$$

The narrow range found for these data suggests that it could be used as a universal constant, which would eliminate the need for frequent plasma analysis. However, it depends on the sensitivity of $CMRO_2$ for its value.

Kinetic Model

Equations 1 and 2 yield

$$\frac{dA_w(t)}{dt} = k \cdot A_t(t) - (k+\lambda) \cdot A_w(t). \qquad \text{Eq. 8}$$

Solving Equation 8 provides the arterial $H_2{}^{15}O$ concentration at a given time, t, in terms of the measured total radioactivity concentration, $A_t(t)$, and a given constant, k (production rate of recirculating water) as:

$$A_w(t) = k \cdot A_t(t) \otimes e^{-(k+\lambda)\cdot t}, \qquad \text{Eq. 9}$$

where $\otimes$ denotes the convolution integral.

If the whole blood curve is already corrected for radioactivity decay of ^{15}O (half-life, 123 sec), the arterial $H_2{}^{15}O$ concentration curve is given as a decay-corrected form:

$$A_w(t) = k \cdot A_t(t) \otimes e^{-k\cdot t}. \qquad \text{Eq. 10}$$

Since the appearance of recirculating water is expected to be delayed due to the circulation time in the body, the arterial $H_2{}^{15}O$ curve, $A_w(t)$, has to be shifted (delayed) from Equation 10:

$$A_w(t) = k \cdot A_t(t - \Delta t) \otimes e^{-k\cdot t}, \qquad \text{Eq. 11}$$

where Δt denotes an average delay time of $H_2{}^{15}O$ appearance, which was assumed to be 20 sec.

Analysis of $^{15}O_2$ PET Data

To evaluate the validity of the present method, $CMRO_2$ and CBF were calculated using the present model and were compared with values obtained from frequent plasma separation.

Following an inhalation of $^{15}O_2$, the radioactivity concentration in a small element of the brain is expressed as a sum of three components (*1–7*): (a) brain tissue radioactivity as a response to supply of $^{15}O_2$, (b) brain tissue radioactivity as a response to supply of $H_2{}^{15}O$ and (c) radioactivity in the blood volume. According to the formulation introduced by Mintun et al. (*1*), the radioactivity concentration is expressed as:

$$R(t) = K_1^o \cdot A_o(t) \otimes e^{-(k_2^w + \lambda)\cdot t} + K_1^w \cdot A_w(t) \otimes e^{-(k_2^w + \lambda)\cdot t} + V_B \cdot 0.85 \cdot \left(1 - 0.835 \cdot \frac{K_1^o}{K_1^w}\right) \cdot A_t(t), \quad \text{Eq. 12}$$

where 0.85 is the peripheral-to-central hematocrit ratio and 0.835 is a fraction of the capillary and venous component in the total blood volume. K_1^o and K_1^w correspond to regional $CMRO_2$ and CBF per given volume of region of interest (ROI) (ml/min/ml), respectively. In this formulation, the first-pass extraction fraction of water has been assumed to be unity. To complement this analysis, cerebral blood volume (CBV, V_B) was measured using the ^{15}O-labeled carbon monoxide scan (*17*), and the distribution volume of water ($V_d = K_1^w/k_2^w$) was measured using a dynamic $H_2{}^{15}O$ scan at rest (see the next section) so that k_2^w in Equation 12 was replaced by K_1^w divided by V_d. K_1^o and K_1^w then were calculated by fitting the measured brain time-activity curve to Equation 12. The arterial $H_2{}^{15}O$ concentration, $A_w(t)$, was simulated by the present model using the whole blood concentration, $A_t(t)$. To validate this method, the $A_w(t)$ curve was also measured by separating the plasma during the $^{15}O_2$ study (*13*) as:

$$A_w(t) = A_{plasma}(t) * R, \quad \text{Eq. 13}$$

where $A_{plasma}(t)$ denotes plasma radioactivity concentration during the $^{15}O_2$ scan, R is the whole blood-to-plasma concentration ratio during the $C^{15}O_2$ inhalation scan, which was measured by one point blood sampling at the end of continuous withdrawal of arterial blood. Here, delay and dispersion in the $A_{plasma}(t)$ curve were carefully corrected as described later.

The arterial $^{15}O_2$ concentration curve, $A_o(t)$, was calculated as (13):

$$A_o(t) = A_t(t) - A_w(t). \quad \text{Eq. 14}$$

Errors in K_1^o and K_1^w estimates due to ambiguity of the assumed k and Δt values in this modeling approach were calculated by using a typical set of data. Both K_1^o and K_1^w were calculated by the fit described above by varying values of either k or Δt, after which %change in the calculated K_1^o and K_1^w values were estimated.

Analysis of $H_2{}^{15}O$ PET Data

A dynamic $H_2{}^{15}O$ administration ($C^{15}O_2$ inhalation) PET scan was performed to determine regional distribution volume of water ($V_d = K_1^w/k_2^w$) (*18*). According to the Kety-Schmidt single-compartment model (*19*), the radioactivity concentration in a small element of the brain following an intravenous injection of $H_2{}^{15}O$ is expressed as:

$$R(t) = K_1^w \cdot A(t) \otimes e^{-(k_2^w + \lambda)\cdot t}, \quad \text{Eq. 15}$$

where A(t) is the whole blood concentration time-activity curve measured by the beta probe, which has already been corrected for delay and dispersion occurring in the tube system and in the internal arterial lines (see below). A pair of K_1^w and V_d ($= K_1^w/k_2^w$) were calculated in terms of nonlinear least squares fitting by fitting the dynamic $H_2{}^{15}O$ data to Equation 15 (*18*). The calculated V_d values were then used in the analysis for dynamic $^{15}O_2$ PET data as described above.

MATERIALS AND METHODS

PET Study

Subjects consisted of four healthy male volunteers, 35–50 yr old (mean ± s.d., 41 ± 7). Following a 10-min transmission scan to correct for attenuation of annihilation photons in the body, a static scan was initiated at 1 min after a $C^{15}O$ inhalation of 7 min to measure cerebral blood volume (V_B in the Equation 10) (*1,20*). Following a 15-min period to allow for the decay of ^{15}O radioactivity in the brain to a background level, a dynamic PET scan was performed following $C^{15}O_2$ inhalation during resting conditions (eyes closed and listening to a 1.5 Hz metronome). The $C^{15}O_2$ gas is equivalent to a $H_2{}^{15}O$ intravenous infusion, since ^{15}O contained in $C^{15}O_2$ gas is exchanged in the lung to $H_2{}^{15}O$ (*21*). The scan was started 30 sec prior to the start of radioactivity delivery and lasted for a total of 4.5 min. The inhalation period was 1 min. The scan sequence consisted of a 30-sec background scan followed by six 5-sec, fifteen 10-sec, and three 30-sec scans.

Two additional dynamic PET scans were obtained while inhaling $^{15}O_2$. The first scan was obtained at rest while listening to the metronome and the second scan during motor activation (finger opposition movement in unison with the metronome). The same scanning sequence described above was employed. The inhalation period for $^{15}O_2$ was 1.5 min.

Arterial blood was continuously withdrawn from the radial artery during dynamic $C^{15}O_2$ and $^{15}O_2$ scanning using a peristaltic pump with a withdrawal speed of 5 ml/min (Fig. 1). A beta probe was used to continuously monitor whole blood radioactivity concentration for both the $^{15}O_2$ scan $\{A_t(t)\}$ and the $C^{15}O_2$ scan $\{A(t)\}$. During $C^{15}O_2$ scanning, the blood derived by the peristaltic pump was collected over 30-sec intervals by changing the sampling tubes. Whole blood concentrations were measured using a well counter that was cross-calibrated to the PET scanner. During $^{15}O_2$ scanning, these samples were immediately centrifuged and their plasma concentrations measured.

The ECAT 931-08/12 tomograph (CTI Inc., Knoxville, TN) was used (*22*). Images were reconstructed to provide an in-plane spatial resolution of 8.4 ± 0.7 mm FWHM at the center of the field of view.

For each subject, a region of interest (ROI) was selected on the primary motor cortex region, which covered two different slices of the PET images. The ROI was defined manually and the number of pixels included in the ROI (pixel size = 2 × 2 mm^2) was 251 ± 32 (mean ± s.d.). ROIs were projected on the static $C^{15}O$ image to calculate CBV values (V_B) as well as dynamic $C^{15}O_2$ and $^{15}O_2$ time frames to produce $C^{15}O_2$ and $^{15}O_2$ time-activity curves. The $C^{15}O_2$ time-activity curves were used to calculate V_d and K_1^w by fitting Equation 15; the $^{15}O_2$ time-activity curves were used to calculate K_1^o and K_1^w by fitting Equation 12.

Correcting the Beta Probe Curve for Delay and Dispersion

Whole blood radioactivity concentration curves measured by the beta probe during $C^{15}O_2$ and $^{15}O_2$ scanning were deconvolved

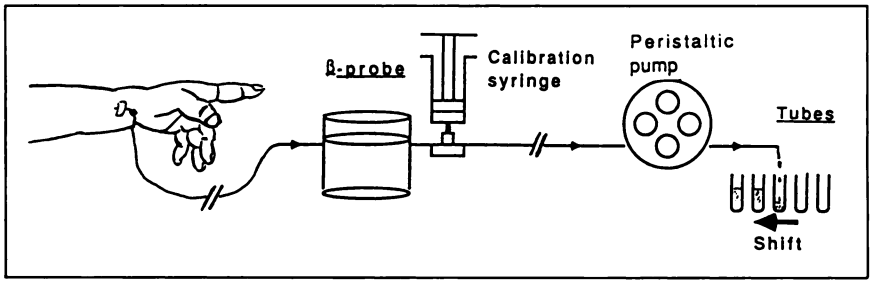

FIGURE 1. A system for measuring the input functions in the $^{15}O_2$ inhalation PET study. Arterial blood is withdrawn from the radial artery using the peristaltic pump. Whole blood radioactivity concentration is continuously monitored to detect beta rays with a plastic scintillator (the beta probe). A syringe sample is taken at the end of the PET scan to calibrate the beta probe curve to the well counter which has been cross-calibrated to the PET scanner prior to the study. The blood from the peristaltic pump is collected every 30 sec by plastic tubes, and these samples are immediately centrifuged to measure the plasma radioactivity concentration. To estimate the delay and dispersion between the beta probe and the tube sampling system, whole blood samples are counted during the $H_2{}^{15}O$ study (see Fig. 2).

by a single exponential function with a fixed dispersion time constant of 5 sec. This is the correction for dispersion (*10*) as measured independently for our constant withdrawal detector system from the catheter to the detector. Further deconvolution was done with a fixed dispersion constant of 4 sec, which corresponded to the correction for relative difference in dispersion between the left ventricle to the radial artery and the left ventricle to the brain (*18*).

The whole grey matter time-activity curve was obtained from the dynamic $H_2{}^{15}O$ data by selecting a ROI for whole grey matter regions in whole slices. Beta probe curve delay in comparison with radiotracer appearance in the brain was adjusted according to a method previously reported (*11*). Briefly, the whole brain curve was described by a single compartment model using the dispersion-corrected beta probe curve and three parameters: the influx and outflux rate constants and delay. The delay plus the influx and outflux rate constants were fitted with nonlinear least squares minimization. Thus, the dispersion, deconvolved beta probe curve, corrected for delay, was used as the true input function for the dynamic $H_2{}^{15}O$ PET study. The same correction factors (delay value and the dispersion time constant) were also used in order to correct for delay and dispersion during the $^{15}O_2$ study.

Correcting the Tube Sampling Curve for Delay and Dispersion

The blood collected by the serial sampling system was counted using the well counter to measure whole blood radioactivity concentration during the $H_2{}^{15}O$ study and plasma concentration during the dynamic $^{15}O_2$ study. Delay and dispersion were determined by comparing the $H_2{}^{15}O$ whole blood concentration curve with the beta probe curve already corrected for delay and dispersion. The corrected beta probe curve was then convolved with a single exponential function with various dispersion time constants and shifted with various delay values. One pair of values (dispersion time constant and delay) was fitted to the tube sampling $H_2{}^{15}O$ whole blood curves by nonlinear least squares minimization. The calculated values of the dispersion time constant were then used to deconvolve the plasma concentration curve to correct for dispersion; the calculated curve was shifted using the obtained delay value which corresponded to the delay correction.

RESULTS

Figure 2 shows an example of a comparison of the whole blood radioactivity curves obtained from a typical $H_2{}^{15}O$ study. The tube's sampling system is explained by the simulated blood curve, which corresponds to the delay and dispersion corrected beta probe curve). The values for the dispersion time constant and the delay calculated in each study were 14 ± 2 and 15 ± 5 sec, respectively. These

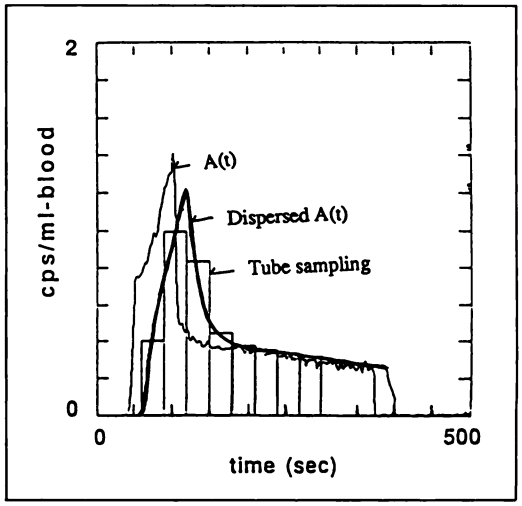

FIGURE 2. Comparison of whole blood radioactivity concentration curves obtained from a typical $H_2{}^{15}O$ study. Histogram denotes the curve obtained by the tube sampling system. The thin solid line corresponds to the beta probe curve in which the dispersion occurring in both the catheter tube (from the catheter to the beta detector) and the internal arteries was corrected together with delay as described in the text. The bold solid line corresponds to the simulated curve by fitting the tube sampling curve (histogram) to the beta probe curve in which delay and dispersion are added to the beta probe curve (thin solid line) to explain the histogram by least squares minimization. The dispersion time constant was calculated as 13 sec when approximating the dispersion function by a single exponential function. The 15-sec delay in this case and these values (delay and dispersion) are used to correct for the delay and dispersion in the plasma concentration curve during the $^{15}O_2$ inhalation study. This calculation is performed for each subject.

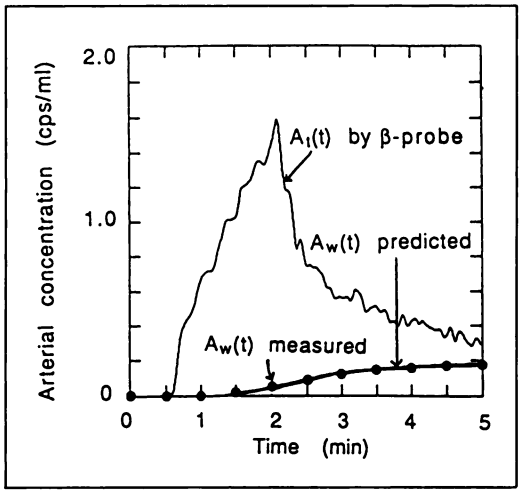

FIGURE 3. Comparison of arterial $H_2{}^{15}O$ concentration curves obtained from a typical $^{15}O_2$ inhalation study. All curves were already corrected for radioactivity decay of ^{15}O. The $A_w(t)$ curve, (bold solid line) was simulated in the present model (Equation 6) using the whole blood concentration curve (thin solid line). This simulated curve agreed well with that measured by frequent plasma separation (closed circles). The whole blood concentration curve was measured using the beta probe, in which delay and the dispersion were corrected as described in the text. The measured $A_w(t)$ curve was obtained using the tube sampling system in which the delay and dispersion included in this measurement system were corrected for using values obtained by the analysis described in Figure 2.

values were used for the delay and dispersion correction in the plasma separation system as described in Methods.

Figure 3 shows the comparison of arterial $H_2{}^{15}O$ concentration curves, $A_w(t)$, obtained from a typical $^{15}O_2$ inhalation study. The $A_w(t)$ curve simulated by the present model (Equation 11) was in good agreement with that measured by frequent plasma separation.

Figure 4 shows the percent difference between measured and simulated $A_w(t)$ for all $^{15}O_2$ studies (eight runs for four subjects) as a function of time following $^{15}O_2$ inhalation. The difference is relatively large during the early phase, whereas $A_w(t)$ concentration is small, but is reduced during later phase, whereas $A_w(t)$ is increased. As summarized in Table 2, integrations of $A_w(t)$ curves (integration over the first 4 min following $^{15}O_2$ inhalation) simulated by the present method agreed well with those measured by frequent plasma separation. The difference was on average (±1 s.d.) 0.9% ± 4.1% (max. 6.5%). These observations suggest the validity of the present model. Moreover, we confirmed that this method predicted the arterial $H_2{}^{15}O$ metabolite concentration curve using the whole blood radioactivity concentration.

TABLE 2
Percent Difference of Integrated Counts Between Measured and Simulated $H_2{}^{15}O$ Curves

Subject	Rest (%)	Activation (%)
RF	5.7	3.4
TF	6.5	1.0
KK	−2.7	0.3
RSJF	−5.1	−2.1
Average ± s.d.	0.9 ± 4.1	(n = 8)

The integration period was 4 min after the start of $^{15}O_2$ inhalation.

Table 3 summarizes results from PET data analysis for the primary motor cortex region of each subject. Values of K_1^o and K_1^w calculated by fitting the $^{15}O_2$ dynamic data using the simulated $A_w(t)$ curve agreed well with those obtained using the measured $A_w(t)$ curve for both resting and activated conditions. Differences in K_1^o and K_1^w were 1.4% ± 1.5% and −1.1% ± 3.6%, respectively.

Errors in the K_1^o and K_1^w estimates due to errors in the assumed delay time, Δt, and the rate constant, k, were plotted in Figure 5. A change in k by ±10% corresponded

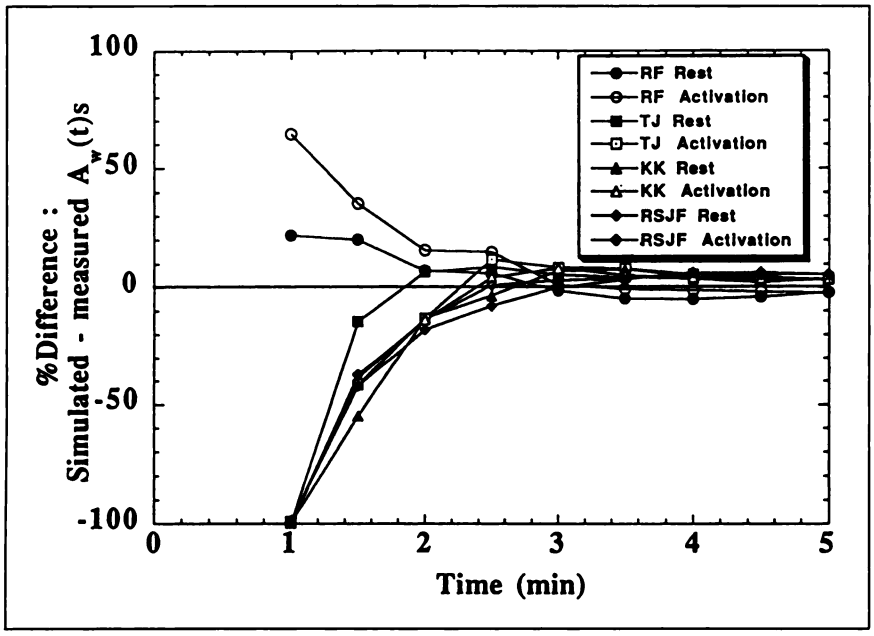

FIGURE 4. Percent differences of simulated $A_w(t)$ curves compared with measured $A_w(t)$ curves by frequent plasma separation as a function of time following $^{15}O_2$ inhalation. Data are plotted for all eight runs performed on four volunteers.

TABLE 3
Results of Analyses on Dynamic $H_2{}^{15}O$ and $^{15}O_2$ PET Data in the Primary Motor Cortex Region at Rest and During Motor Activation (Finger Opposition)

	Subject					
	RF	TJ	KK	RSJF	Mean	±s.d.
Hb	12.9	14	14.8	15.4	14.3	1.1 (g/100 ml)
PaO_2	99	99.75	97.5	82.5	94.7	8.2 (mmHg)
$PaCO_2$	38.25	39.75	45.75	45	42.2	3.7 (mmHg)
Results of $C^{15}O$ scan						
CBV	0.025	0.035	0.031	0.033	0.031	0.005 (ml/g)
Results of $H_2{}^{15}O$ fitting						
K_1^w at rest	0.536	0.422	0.494	0.541	0.498	0.055 (ml/min/ml)
V_d at rest	0.872	0.791	0.742	0.771	0.794	0.056 (ml/min)
Results of $^{15}O_2$ fitting (recirculating water predicted by the present method)						
K_1^o at rest	0.244	0.214	0.194	0.191	0.211	0.024 (ml/min/ml)
K_1^w at rest	0.489	0.430	0.506	0.560	0.496	0.054 (ml/min/ml)
K_1^o during activation	0.269	0.233	0.215	0.198	0.229	0.030 (ml/min/ml)
K_1^w during activation	0.629	0.501	0.635	0.650	0.604	0.069 (ml/min/ml)
Increase in K_1^o	10.2	8.9	10.8	3.7	8.4	3.3 (%)
Increase in K_1^w	28.6	16.5	25.5	16.1	21.7	6.4 (%)
Results of $^{15}O_2$ fitting (recirculating water measured by frequency plasma separation)						
K_1^o at rest	0.240	0.214	0.189	0.188	0.208	0.025 (ml/min/ml)
K_1^w at rest	0.504	0.419	0.497	0.567	0.497	0.061 (ml/min/ml)
K_1^o during activation	0.267	0.236	0.210	0.192	0.226	0.033 (ml/min/ml)
K_1^w during activation	0.684	0.517	0.624	0.646	0.618	0.072 (ml/min/ml)
Increase in K_1^o	11.3	10.3	11.1	2.1	8.7	4.4 (%)
Increase in K_1^w	35.7	23.4	25.6	13.9	24.6	8.9 (%)
%Difference between the two methods						
K_1^o at rest	1.7	0.0	2.6	1.6	1.5	1.1 (%)
K_1^w at rest	−3.0	2.6	1.8	−1.2	0.1	2.6 (%)
K_1^o during activation	0.7	−1.3	2.4	3.1	1.2	1.9 (%)
K_1^w during activation	−8.0	−3.1	1.8	0.6	−2.2	4.4 (%)
K_1^o rest + activation					1.4	1.5 (%)
K_1^w rest + activation					−1.1	3.6 (%)

to an error of ±3% and 6% in the K_1^o and K_1^w estimates, respectively. A change in the delay by ±10 sec (Δt = 10 and 30 sec) corresponded to differences in K_1^o and K_1^w of ±2% and 4%, respectively.

DISCUSSION

Our model reproduces an arterial metabolite concentration curve using only the whole blood radioactivity concentration in $^{15}O_2$ inhalation PET so that plasma separation can be avoided. The procedure needed to measure the plasma radioactivity concentration curve is not simple enough for a clinical use. This is confounded by the fact that corrections for delay and dispersion in the measured plasma radioactivity curve are not straightforward and several procedures are required. The present approach provides arterial $H_2{}^{15}O$ and $^{15}O_2$ concentration curves by only measuring the whole blood radioactivity concentration curve with a beta probe.

Previous workers assumed that the $A_w(t)$ curve increased linearly during the first part of data acquisition, and linear interpolation has been used between the scan start time and the plasma sampling time (*1*). This assumption may be valid if the total PET scan period is short enough. However, for a longer scan time such as the present protocol for determining $CMRO_2$ and CBF with dynamic PET, the accuracy of linear interpolation might be limited (Fig. 3). Several samples needed to be taken to obtain an accurate $A_w(t)$ curve.

Three main assumptions were made from the present model:

1. Production of $H_2{}^{15}O$ from $^{15}O_2$ follows a single rate constant model.
2. The rate constant can be fixed using the value from the ratio of whole blood and plasma obtained from 200 steady-state studies.
3. The delay of $H_2{}^{15}O$, due mainly to recirculation time in the body, can be fixed.

The first assumption may not be strictly valid because release of $H_2{}^{15}O$ must be composed of many rate constants corresponding to various extraction ratios and blood flow for specific body organs. However, we demonstrate (Figs. 3 and 4) the empirical validity of our simplified model for clinical use. The second and the third assumptions might be valid only for a slow inhalation protocol. It should be noted that $^{15}O_2$ was inhaled for 1.5 min in this study and that the total PET scanning time was 4 min after starting the inhalation. If $^{15}O_2$ is inhaled as a bolus, the recirculating water in arterial blood will be a proportionately greater component than that observed in Figure 3. The $A_w(t)$ curve

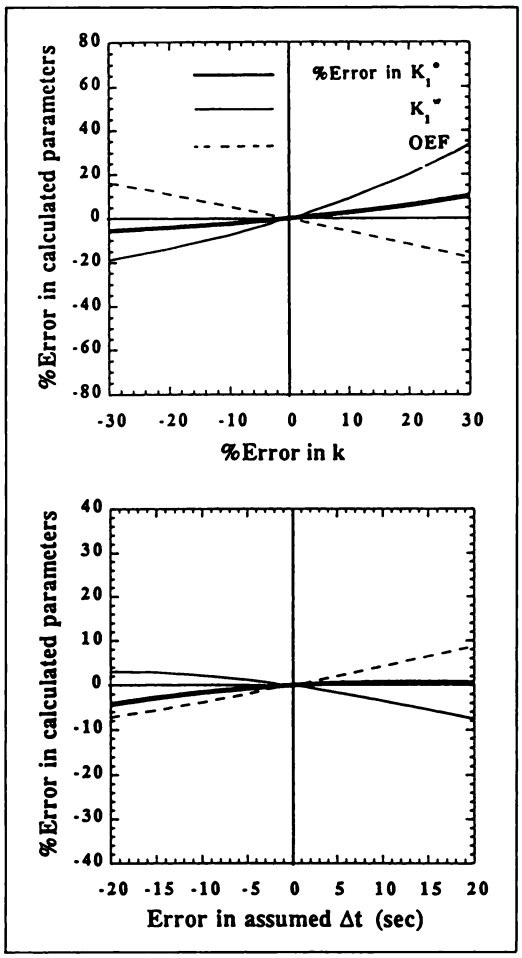

FIGURE 5. Error sensitivity to assumed values of k and Dt in K_1^o and K_1^w estimates. K_1^o, K_1^w and oxygen extraction fraction (OEF $\int K_1^w/K_1^o$) were calculated by varying the assumed values of k and Dt for a typical set of data (subject RSJF at rest). The %difference in the K_1^o and K_1^w estimates were plotted as a function of %error in k (upper) and change of Δt (lower). Bold solid lines, thick solid lines and dashed lines correspond to errors in K_1^o, K_1^w and OEF, respectively.

is probably more variable between subjects, and there may thus be greater error with the bolus inhalation protocol. A slow inhalation protocol is therefore recommended in order to minimize errors with this method.

Huang et al. (*23*) have developed a three-compartment model to describe the time-course of recirculating water following $^{15}O_2$ inhalation. They obtained a conversion rate constant of recirculating water in arterial blood from six human studies of 0.131 ± 0.026 (1/min). The significant difference of their rate constant from our value (k = 0.0722 ± 0.0126 [1/min]) was probably due to the difference of the model (i.e., the third compartment which may correspond to absorption of metabolized water in the body was included in their model).

A noninvasive measurement of arterial whole blood radioactivity concentration may be possible in the future by using small detectors to scan the radial artery (*24*) or by using an additional PET scanner to measure radioactivity concentration in the cardiac chamber (*25*). The present model will be applicable for calculating input functions (arterial $H_2{}^{15}O$ and $^{15}O_2$ concentration curves) needed in $^{15}O_2$ analysis using the whole blood radioactivity concentration curve. Arterial O_2 content may be estimated within a certain degree of accuracy from a measurement of hemoglobin content of venous blood and an assumption of oxygen saturation in the arterial blood. For instance, the variation in PaO_2 in our subject group (from 82.5 to 99 mmHg) corresponds to the variation of the oxygen saturation of only a few percent at normal temperatures and normal pH.

The same principle described in this article (Equation 1) may be valid for predicting arterial metabolites using the whole blood radioactivity curve for PET studies with various compounds, especially if data are available from prior metabolite analysis studies of patient populations with the equilibrium value of the ratio between labeled parent and metabolite. Application of Equation 1 may also be possible for predicting the plasma radioactivity concentration curve from the whole blood radioactivity curve in ^{18}F-fluorodeoxyglucose PET studies. Further study is needed to evaluate these claims.

In conclusion, we employed a method which simultaneously calculates $CMRO_2$ and CBF from a $^{15}O_2$ inhalation dynamic PET scan with given values of CBV and V_d. An advantage of this method is that a measurement of CBF, as required for each physiological condition in Mintun's method (*1*), is not required here. Error sensitivity analysis also demonstrated that this method was not sensitive to changes in CBV, and hence CBV can be measured by a $C^{15}O$ inhalation scan during at rest. Thus, once a dynamic $H_2{}^{15}O$ PET scan (for V_d measurement) and a $C^{15}O$ inhalation scan are performed at rest, both $CMRO_2$ and CBF can be calculated simultaneously for various physiological conditions from a single dynamic $^{15}O_2$ PET scan.

We also observed increased CBF and $CMRO_2$ during finger movement in all subjects. However, it has been shown that an increase in $CMRO_2$ was always less than that in CBF by a factor of approximately 1/3. This observation is consistent with previous findings of the uncoupling between CBF and $CMRO_2$ during neuronal activation, although the magnitude of the increase in $CMRO_2$ was somewhat greater in this study. Further study is required to evaluate the significance of this observation.

ACKNOWLEDGMENTS

The authors thank Dr. Adriaan A. Lammertsma from the MRC Cyclotron Unit, Hammersmith Hospital, London, U.K. for invaluable discussions as well as the MRC Cyclotron Unit staff—particularly, Messrs. Peter Bloomfield, John Ashburner and Jon D. Heather for computer assistance; Miss Claire J.V. Taylor and Mr. Graham Lewington for technical support; and Drs. Henri Tochon-Danguy, Patricia Landais and Colin Steel for preparing radioactivity gases. HI was supported by the Japan Heart Foundation and a 1988 Bayer Yakuhin grant.

REFERENCES

1. Mintun MA, Raichle ME, Martin WRW, Herscovitch P. Brain oxygen utilization measured with O-15 radiotracers and positron emission tomography. *J Nucl Med* 1984;25:177–187.
2. Meyer E, Tyler JL, Thompson CJ, Redies C, Diksic M, Hakim AM. Estimation of cerebral oxygen utilization rate by single bolus $^{15}O_2$ inhalation and dynamic positron emission tomography. *J Cereb Blood Flow Metab* 1987;7:403–414.
3. Holden JE, Eriksson L, Roland PE, Stone-Elander S, Widen L, Kesselberg M. Direct comparison of single-scan autoradiographic with multiple-scan least-squares fitting approaches to PET $CMRO_2$ estimation. *J Cereb Blood Flow Metab* 1988;8:671–680.
4. Huang S-C, Feng D-G, Phelps ME. Model dependency and estimation reliability in measurement of cerebral oxygen utilization rate with oxygen-15 and dynamic positron emission tomography. *J Cereb Blood Flow Metab* 1986;6:105–119.
5. Iida H, Jones T, Deiber MP, Cunningham V, Frackowiak RSJ. Simultaneous measurement of CMRO2 and CBF using a slow inhalation of $^{15}O_2$ and dynamic PET [Abstract]. *J Nucl Med* 1990;31:760.
6. Iida H, Jones T, Frackowiak RSJ. Simultaneous measurement of CBF and $CMRO_2$ by single dynamic PET scanning with use of $^{15}O_2$. *J Cereb Blood Flow Metab* 1991;11(suppl):S579.
7. Lammertsma AA, Frackowiak RSJ, Hoffman JM, Huang SC, Weinberg I, Phelps ME. Simultaneous measurement of regional cerebral blood flow and oxygen metabolism: a feasibility study. *J Cereb Blood Flow Metab* 1987; 7(suppl):S587. [Abstract]
8. Daghighian F, Huang SC, Hoffman JM, et al. Measurement of $lCMRO_2$ and CBF with O_2 dynamic PET using on-line plasma separation for input function [Abstract]. *J Nucl Med* 1989;30:791.
9. Chen BC, Huang SC, Daghighian F, et al. Parametric imaging of the cerebral oxygen metabolic rate (CMRO2) using dynamic PET and on-line plasma separator. *J Cereb Blood Flow Metab* 1991;11(suppl 2):577. [Abstract]
10. Iida H, Kanno I, Miura S, Murakami M, Takahashi K, Uemura K. Error analysis of a quantitative cerebral blood flow measurement using $H_2{}^{15}O$ autoradiography and positron emission tomography with respect to the dispersion of the input function. *J Cereb Blood Flow Metab* 1986;6:536–545.
11. Iida H, Higano S, Tomura N, et al. Evaluation of regional differences of tracer appearance time in cerebral tissues using ^{15}O-water and dynamic positron emission tomography. *J Cereb Blood Flow Metab* 1988;8:285–288.
12. Iida H, Jones T, Miura S. Modeling approach to eliminate the plasma separation in $^{15}O_2$ inhalation PET. *J Cereb Blood Flow Metab* 1991;11(suppl 2):S578.
13. Lammertsma AA, Correia JA, Jones T. Stability of arterial concentrations during continuous inhalation of $C^{15}O_2$ and $^{15}O_2$ and the effects on computed values of CBF and $CMRO_2$. *J Cereb Blood Flow Metab* 1988;8:411–417.
14. Jones T, Chesler DA, Ter-Pogossian MM. The continuous inhalation of oxygen-15 for assessing regional oxygen extraction in the brain of man. *Br J Radiol* 1976;49:339–343.
15. Subramanian R, Alpert NM, Hoop B Jr, Brownell GL, Taveras JM. A model for regional cerebral blood oxygen distribution during continuous inhalation of $^{15}O_2$, $C^{15}O$ and $C^{15}O_2$. *J Nucl Med* 1978;19:48–53.
16. Frackowiak RSJ, Lenzi GL, Jones T, Heather JD. Quantitative measurement of regional cerebral blood flow and oxygen metabolism in man using O-15 and positron emission tomography: theory, procedure, and normal values. *J Comput Assist Tomogr* 1980;4:727–736.
17. Lammertsma AA, Jones T. Correction for the presence of intravascular oxygen-15 in the steady-state technique for measuring regional oxygen extraction ratio in the brain: 1. Description of the method. *J Cereb Blood Flow Metab* 1983;3:416–424.
18. Iida H, Kanno I, Miura S, Murakami M, Takahashi K, Uemura K. A determination of the regional brain/blood partition coefficient of water using dynamic positron emission tomography. *J Cereb Blood Flow Metab* 1989; 9:874–885.
19. Kety SS. The theory and applications of exchange of inert gas at the lungs and tissues. *Pharmacol Res* 1951;3:1–41.
20. Grubb RJ Jr, Raichle ME, Higgins CS, et al. Measurement of regional cerebral blood volume by emission tomography. *Ann Neurol* 1978;4:322–328.
21. West JB. *Respiratory physiology—the essentials*. Baltimore: Williams & Wilkins Co.; 1979:74.
22. Spinks TJ, Jones T, Gilardi MC, Heather JD. Physical performance of the latest generation of commercial positron scanner. *IEEE Trans Nucl Sci* 1988;35:721–725.
23. Huang SC, Barrio JR, Yu DC, et al. *Phys Med Biol* 1991;36:749–761.
24. Rajeswaren SR, Hume SP, Townsend DW, Geissbuhler A, Jones T. A new design for a dedicated small animal PET scanner. *J Cereb Blood Flow Metab* 1991;11(suppl 2):S566. [Abstract]
25. Iida H, Rhodes CG, Kanno I, Jones T, Silva RD, Araujo LA. Noninvasive LV time-activity curve as an input function in $H_2{}^{15}O$ dynamic PET. *J Nucl Med* 1992;32:1669–1677.